

Angular momentum loss of primordial gas in Ly α radiation field

Hidenobu Yajima^{1,2,3*} and Sadegh Khochfar¹

¹ SUPA \dagger , Institute for Astronomy, University of Edinburgh, Royal Observatory, Edinburgh, EH9 3HJ, UK

² Department of Astronomy and Astrophysics, Pennsylvania State University, 525 Davey Lab, University Park, PA 16802, USA

³ Institute for Gravitation and the Cosmos, The Pennsylvania State University, University Park, PA 16802, USA

Accepted ?; Received ??; in original form ???

ABSTRACT

We present results on the radiation drag exerted by an isotropic and homogenous background of Ly α photons on neutral gas clouds orbiting within HII regions around Population III stars of different masses. The Doppler shift causes a frequency difference between photons moving in the direction of the cloud and opposite to it resulting in a net momentum loss of the cloud in the direction of motion. We find that half of the angular momentum of gas with $v_\theta \lesssim 20 \text{ km s}^{-1}$ near ($r \lesssim 3 \text{ kpc}$) a Population III star of $120 M_\odot$ at $z = 20$ is lost within $\sim 10^6 \text{ yr}$. The radiation drag is a strong function of cloud velocity that peaks at $v \sim 20 \text{ km s}^{-1}$ reflecting the frequency dependence of the photon cross section. Clouds moving with velocities larger than $\sim 100 \text{ km s}^{-1}$ lose their angular momentum on time scales of $\sim 10^8 \text{ yr}$. At lower redshifts radiation drag becomes inefficient as the Ly α photon density in HII regions decreases by a factor $(1+z)^3$ and angular momentum is lost on time scales $\gtrsim 10^8 \text{ yr}$ even for low velocity clouds. Our results suggest that a sweet spot exists for the loss of angular momentum by radiation drag for gas clouds at $z > 10$ and with $v \sim 20 \text{ km s}^{-1}$. Comparison to dynamical friction forces acting on typical gas clouds suggest that radiation drag is the dominant effect impacting the orbit. We propose that this effect can suppress the formation of extended gas discs in the first galaxies and help gas accretion near galactic centres and central black holes.

Key words: radiative transfer – galaxies: formation – galaxies: evolution – cosmology: dark ages, reionization, first stars

1 INTRODUCTION

Unraveling the evolution from Population III (Pop III) stars to the first galaxies is an open issue. The key to gain insight into this transition is to understand how gas is accreted onto proto-galaxies and its ability to conserve angular momentum or not. The latter has direct impact on the formation of possible discs (Pawlik et al. 2011; Romano-Díaz et al. 2011), star formation (Khochfar & Silk 2011) or feeding of black hole seeds (Di Matteo et al. 2012; Agarwal et al. 2012, 2013).

In this study, we investigate the angular momentum loss of accreted gas clouds around Pop III stars due to radiation drag by Ly α photons. In an isotropic radiation field, moving gas is exerted to stronger radiation pressure along opposite

sites with respect to the moving direction due to the Doppler shift. A similar effect on dust is classically known as the Poynting-Robertson effect (Poynting 1903; Robertson 1937) and used to explain angular momentum loss of dust in the solar system.

The effect of the radiation drag on primordial gas clouds in the early universe was studied analytically (Loeb 1993) and numerically (Umemura et al. 1993). Loeb (1993) and Umemura et al. (1993) focused on the radiation drag exerted by the cosmic microwave background and suggested angular momentum of gas could efficiently be lost at $z \sim 200$, resulting in supermassive stars under the assumption that stellar source cause cosmic reionization, and that the CMB photons can efficiently be scattered by free electrons.

However, current theoretical work shows Pop III stars form at $z \sim 15 - 20$ followed by the first galaxies at $z \sim 10 - 15$ (e.g., Bromm & Yoshida 2011). The CMB is therefore

* E-mail: yajima@roe.ac.uk (HY)

\dagger Scottish Universities Physics Alliance

no longer a possible source for efficient radiation drag on primordial gas.

In this paper we revisit the effects of radiation drag, in contrast to earlier work focusing on Ly α radiation fields produced by Pop III stars. Unlike in the case for CMB photons, the number density of Ly α photons from Pop III stars can be much higher because they can be locally trapped within HII regions by scattering on their borders. In addition, the cross section near the line centre is quite high $\sim 10^{-14}$ cm 2 (Verhamme et al. 2006), which is ~ 10 orders of magnitude higher than the Thomson scattering cross section. As a result, the orbiting gas clouds in the Ly α radiation fields experience numerous scattering events and are subject to a drag force. However, unlike Compton scattering of continuum radiation, scattering of Ly α photons is very sensitive to the velocity of the cloud. The Doppler shift of the line centre and the strong frequency dependence of the cross section may lead to an only small drag force. In this letter, we study the effect of radiation drag on accreted gas clouds under different physical conditions such as e.g., different stellar masses of Pop III stars, redshifts, and initial velocities of infalling clouds.

Our paper is organized as follows. We describe our model and method to calculate the radiation drag in Section 2. In Section 3, we show the velocity evolution of test gas particles, and show the dependence on stellar mass and redshift. Finally, in Section 4, we summarize our main conclusions and discuss limitations of our model.

2 MODEL

Based on the current standard cold dark matter paradigm, halos grow via merging and accretion. High-density gas entering the HII regions around Pop III stars, which exceeds the virial radius of the halo (Abel et al. 2007), can stay neutral due to self-shielding (e.g., Yajima et al. 2012e), but experience numerous scatter events with Ly α photons (Dijkstra & Kramer 2012; Laursen et al. 2013). The critical density required for such clouds to stay neutral via self-shielding in the vicinity of the Pop III star depends on the flux of stellar radiation seen by these clouds. Following Umemura et al. (2012) we can estimate the threshold density via,

$$\dot{N}_{\text{Ion}}^{\gamma} \frac{\pi r_c^2}{4\pi D^2} < \frac{4\pi r_c^3}{3} \alpha_B n_c^2, \quad (1)$$

where $\dot{N}_{\text{Ion}}^{\gamma}$ is the ionizing photon emissivity of the star, and α_B is the recombination coefficient to all excited levels of hydrogen (Hui & Gnedin 1997), D is the distance between the star and the gas cloud, n_c is the hydrogen number density of the cloud and r_c its radius. In this work, we assume that the gas temperature is 10^4 K in the HII region with $\alpha_B = 2.6 \times 10^{-13}$ cm $^{-3}$ s $^{-2}$ (Hui & Gnedin 1997). The left-side of the above equation is the maximum incident photon number, while the right-hand side is the total recombination rate in an ionized cloud. Using typical parameters and rearranging the threshold density for self-shielding is given

by,

$$n_{\text{th}} = 8.9 \times 10^{-2} \text{ cm}^{-3} \left(\frac{\dot{N}_{\text{Ion}}^{\gamma}}{10^{50} \text{ s}^{-1}} \right)^{\frac{1}{2}} \left(\frac{D}{1 \text{ kpc}} \right)^{-1} \left(\frac{r_c}{100 \text{ pc}} \right)^{-\frac{1}{2}}. \quad (2)$$

The above relation approximates the limiting case of an ionizing front (I-front) not being able to sweep through a neutral gas cloud. Once equilibrium between ionization and recombinations in the cloud is reached, the I-front stalls and ionization balance gives $\dot{N}_{\text{Ion}}^{\gamma} \pi r_c^2 / (4\pi D^2) = V_{\text{HII}} \alpha_B n_c^2$, where V_{HII} is the volume of the ionized region. Taking the volume-weighted neutral fraction (χ_{HI}) of the cloud as $1 - (V_{\text{HII}}/V_c)$ with $V_c = 4\pi r_c^3/3$ as the total volume of the cloud, the neutral fraction becomes $\chi_{\text{HI}} = 1 - \frac{3\dot{N}_{\text{Ion}}^{\gamma}}{16\pi\alpha_B D^2 r_c n_c^2}$. A cloud of $r_c = 100$ pc with densities larger than 0.13 cm $^{-3}$ will stay mostly neutral $\chi_{\text{HI}} \geq 0.5$ at a distance $D = 1$ kpc from a star with $\dot{N}_{\text{Ion}}^{\gamma} = 10^{50}$ s $^{-1}$. This estimate is lower than in the case of ionization equilibrium under the optically thin approximation and same neutral fraction everywhere in the cloud, i.e., $\dot{N}_{\text{Ion}}^{\gamma} \sigma_{\text{Ion}} \chi_{\text{HI}} / (4\pi D^2) = \alpha_B n_c (1 - \chi_{\text{HI}})^2$ where $\sigma_{\text{Ion}} = 6.3 \times 10^{-18}$ cm 2 is the ionization cross section (Osterbrock & Ferland 2006). Under this approximation the above cloud becomes $\chi_{\text{HI}} \geq 0.5$ at densities ≥ 40.7 cm $^{-3}$. However, in realistic situations the ionizing flux diminishes in the cloud and the neutral fraction can be much higher than the estimation under the optically thin approximation and typically deviates from this approximation at $n_c \gtrsim 0.01$ cm $^{-3}$ (Yajima et al. 2012e; Rahmati et al. 2013b), suggesting this estimate to be an upper limit on the density. In addition, the equation 2 can be converted to a column density threshold by multiplying $2r_c$, i.e., $N_{\text{th}} = 5.5 \times 10^{19}$ cm $^{-2}$ ($\dot{N}_{\text{Ion}}^{\gamma}/10^{50}$ s $^{-1}$) $(D/1 \text{ kpc})^{-1} (r_c/100 \text{ pc})^{1/2}$. A cloud of $N_{\text{th}} = 5.5 \times 10^{19}$ cm $^{-2}$ corresponds to a typical Lyman limit system (Prochaska, O’Meara & Worseck 2010), and is mostly optically thick to external UV radiation as shown in recent cosmological simulations (Faucher-Giguère & Kereš 2011; Rahmati et al. 2013a). Hence, clouds with $n > n_{\text{th}}$ are self-shielded against stellar radiation which is also supported by recent radiative-hydrodynamics simulations (Susa & Umemura 2006; Umemura et al. 2012). To estimate whether infalling gas clouds at these high redshifts can indeed stay neutral we consider the case of a cloud in a mini halo being accreted at $z = 20$. Its mean density is $\sim 18\pi^2$ times that of the background (Bryan & Norman 1998), or $n_{\text{H}} = 1.9 \times 10^{-7} \times (1+20)^3 \times 18\pi^2 = 0.3$ cm $^{-3}$. This is larger than the estimated threshold assuming a Pop III star of $120 M_{\odot}$ as the central source, and predicts neutral infall. Further support comes from simulations by Abel et al. (2007) who show that a gas cloud accreted along a cosmic filament does survive photoevaporation even at a distance of 50 pc from the star (see also Umemura et al. 2012). On the other hand, the threshold density is sensitive to the separation to the star. If clouds enter the virial radius, within the life time of stars (~ 3 Myr), for a virial radius of $D \sim 70$ pc (corresponding to a dark matter halo of $\sim 10^5 M_{\odot}$ at $z = 20$) the threshold density gets $n_{\text{th}} = 1.3$ cm $^{-3}$ which is larger than the mean density of the halo. It is therefore likely that some fraction of the infalling clouds, in particular those that come closest to the star on a short time scale, are destroyed

due to the photoevaporation (see also Hasegawa et al. 2009; Susa, Umemura & Hasegawa 2009).

Even after the death of the central star in a HII region, Ly α photons are produced over a recombination timescale ($\tau \sim 6 \times 10^7$ yr at $z=20$), and can be trapped in the residual HII region. As well as Ly α photons, ionizing photons are also emitted by recombination from a halo. The total power of ionizing photons from a halo by recombination is similar to that by stellar sources (e.g., Raičević et al. 2013) leaving infalling clouds neutral due to self-shielding. The recombination time scale of gas in haloes is much smaller than that of the inter-galactic medium (IGM), $\tau \sim 6 \times 10^5$ yr terminating ionizing photons from a halo at almost the same time when the central star dies. Although the production of ionizing photons from the IGM is continuing its emissivity is small due to its low density. At this stage, even lower-density accreted gas can stay neutral because there is no strong ionizing photon contribution and interact with the abundant Ly α photons.

Ly α photons interacting along the direction of motion have larger energies than those opposite to it due to the Doppler shift. This leads to a net momentum loss and drag force in the direction of motion of $\Delta P \sim 2 \times h\nu_0(v/c^2)$, where $\nu_0 = 2.466 \times 10^{15}$ Hz is the frequency of the line centre. Figure 1 shows the schematic view of our model. The drag force is proportional to the number density of Ly α photons locked up within the HII region. In the following paragraphs we derive estimates for the number density of Ly α photons.

We estimate the size of HII regions assuming a uniform inter-galactic medium (IGM) around Pop III stars and neglect the clumpiness of the IGM which has been shown in numerical simulations to be small and $\lesssim 3$ (Pawlik et al. 2009; Paardekoooper et al. 2013). This leads to an estimate of the size of the HII region in equilibrium based on the Strömrgren sphere analysis (Strömrgren 1939) :

$$R_S = \left(\frac{3\dot{N}_{\text{Ion}}^\gamma f_{\text{esc}}}{4\pi\alpha_B n_H^2(z)} \right)^{\frac{1}{3}}, \quad (3)$$

where R_S is the radius of the Strömrgren sphere, $\dot{N}_{\text{Ion}}^\gamma$ is the ionizing photon emissivity of stars, f_{esc} is the escape fraction of ionizing photons from the halo. For small haloes hosting Pop III stars, most of the gas can easily evaporate due to photo-ionization and a large fraction of ionizing photon can escape (Whalen et al. 2004; Kitayama et al. 2004). Note however, that estimates for f_{esc} can vary significantly with halo and stellar mass (Kitayama et al. 2004; Yoshida et al. 2007), and are somewhat dependent on the resolution of the simulation (Yajima et al. 2011; Rahmati et al. 2013b). Here we assume $f_{\text{esc}} = 0.5$ which is supported by recent simulations (Abel et al. 2007; Paardekoooper et al. 2013). The recombination time scale is of order $10^7 - 10^8$ yr and as such longer than the life time of massive Pop III stars resulting in the ionization front being within R_S during the life time of the star (Spitzer 1978),

$$R_I = R_S (1 - \exp(-t_{\text{life}}/\tau_{\text{rec}}))^{1/3}, \quad (4)$$

where t_{life} is life time of the star, $\tau_{\text{rec}} \sim 1/\alpha_B n_H$ is the recombination time-scale, and R_I is the radius of the ionization front. About 0.68 of ionizing photons emitted from stars are converted to Ly α photons via recombinations

(Osterbrock & Ferland 2006). A large fraction of these Ly α photons is scattered at the outer HI layer (Verhamme et al. 2006; Dijkstra & Loeb 2008) and locked inside the HII region, leading to a significant increase in their number density (Yajima & Li 2012a). We estimate the total number of Ly α photons in HII regions as

$$N_{\text{Ly}\alpha} \sim 0.68 \times (1 - f_{\text{esc}}) \times \dot{N}_{\text{Ion}}^\gamma \times t_{\text{trap}}, \quad (5)$$

where t_{trap} is the trapping time of Ly α photons in the HII region. Here, as a fiducial model, we assume for simplicity that $t_{\text{trap}} = t_{\text{life}}$. This model implies that absorbed ionizing photons in haloes convert to Ly α photons via the recombination process and are then stocked in the ionized region. The drag force F_{drag} is proportional to the number density of Ly α photons and thus $F_{\text{drag}} \propto (1 - f_{\text{esc}})/f_{\text{esc}}$ because the ionized regions become smaller as $V_{\text{HII}} \propto f_{\text{esc}}$ and the total Ly α photon number increases with $N_{\text{Ly}\alpha} \propto (1 - f_{\text{esc}})$. Hence, F_{drag} increases as the f_{esc} decreases, while the volume of the trapped Ly α radiation field becomes smaller. The frequency of Ly α photons changes during each scattering event. Typically after an average of $N_{\text{scat}} \sim 0.9\tau_0$ scattering events (Harrington 1973), the Ly α photon frequency changes to frequencies with low cross sections and they escape from the previously optically thick medium. In the case of outflowing gas like the IGM, only photons at longer wavelength than ν_0 can travel for long distances (Loeb & Rybicki 1999; Laursen et al. 2009; Yajima et al. 2012b). On the other hand, for circumgalactic gas that is infalling only photons at shorter wavelengths can escape from the local region (Yajima et al. 2012c). If we consider an outflow paralleling the Hubble flow, the optical depth for the IGM is $\tau_0 \sim 10^6$. Under such circumstances Ly α photons are efficiently scattered at the outer HI layer (Verhamme et al. 2006; Dijkstra & Loeb 2008; Yajima & Li 2013). The trapping time of Ly α photons (t_{trap}) in HII regions can be much longer than the life time of Pop III stars $\sim 10^6$ yr (Schaerer 2002) by $t_{\text{trap}} \sim 0.9\tau_0 \times 2R_I/c \gtrsim 10^{10}$ yr, here we use $R_I \sim 2.9$ kpc representative for a Pop III star with $120 M_\odot$ at $z = 20$. Hence, all emitted Ly α photons from haloes can be locked within the HII region. This estimate is an upper limit, as some fraction can enter into the HI layer and escape. Please note that even after a star dies, the recombination processes in the residual HII region keeps producing Ly α and ionizing photons. The total number of Ly α photons continues increase during this time due to the trapping effect, while ionizing photons are destroyed via absorption by hydrogen and recombination to excited levels. In this work we use a constant value for the density of Ly α photons based on Eq.5. However, the trapping time becomes shorter in the recombining IGM. Adams (1975) derived the trapping time in spherical uniform and plane-parallel clouds. He showed $t_{\text{trap}} \sim 15t_{\text{cross}}$ for $3 < \log\tau_0 < 6$, where τ_0 is the optical depth of the Ly α line centre and t_{cross} is the crossing time of photons through a system of size L , i.e., $t_{\text{cross}} = L/c$. To account for this we also study cases with lower photon densities with $t_{\text{trap}} = 15t_{\text{cross}}$ with $t_{\text{cross}} = 2R_I/c$. The number density of Ly α photons in the HII is then estimated by $n_{\text{Ly}\alpha} = N_{\text{Ly}\alpha}/V_{\text{HII}} = 3N_{\text{Ly}\alpha}/4\pi R_I^3$.

In our model we assumes a spherical symmetric HII region. Depending on the environment and physical situation, geometries in general can vary from highly non-symmetric (Abel et al. 2007) to spherical (Yoshida et al. 2007). How-

ever, the number density of Ly α photons is dominated by the ionizing photon emissivity from the central star and the volume of HII region as explained above. It is not sensitive to the detailed shape of the HII region. We further assume a homogeneous Ly α radiation field in the HII region. In practice, since Ly α photons are emitted from high-density gas within the halo, the Ly α photon density increases towards the halo. However, due to the photon trapping effect and the associated scattering of Lyman-alpha photons into random directions within the HII region, the cumulative number of Ly α photons is much higher than the in situ emission from the halo and the Ly α radiation field becomes highly homogeneous.

For convenience, in what follows we introduce a variable $x \equiv (\nu - \nu_0)/\Delta\nu_D$, where $\Delta\nu_D = [2k_B T/(m_p c^2)]^{1/2} \nu_0$. The intensity can then be expressed as,

$$I(x) = I_0 H(a, x), \quad (6)$$

where

$$I_0 = \frac{n_{\text{Ly}\alpha} c}{4\pi \int dx H(a, x)}, \quad (7)$$

and $a = \Delta\nu_L/(2\Delta\nu_D)$ is the relative line width with the natural line width $\Delta\nu_L = 9.936 \times 10^7$ Hz, and $H(a, x)$ is the Voigt function (Verhamme et al. 2006),

$$H(a, x) = \frac{a}{\pi} \int_{-\infty}^{+\infty} \frac{e^{-y^2}}{(x-y)^2 + a^2} dy \sim \begin{cases} e^{-x^2} & \text{if } |x| < x_c \\ \frac{a}{\sqrt{\pi} x^2} & \text{if } |x| > x_c, \end{cases} \quad (8)$$

where x_c is the boundary frequency between a central resonant core and the power-law ‘‘damping wings’’. We use the fitting formula by Tasitsiomi (2006) which can reproduce the Voigt function smoothly even at $x \sim x_c$. During each scattering event, the frequency of Ly α photons changes. However, when the optical depth of the IGM is high, a very small fraction of Ly α photons at the wing part of the distribution can escape from local regions. Hence, the line profile in HII region stays a Voigt function. Furthermore, the propagation of I-front does not accompany high-velocity motion of gas (Yoshida et al. 2007). Therefore, the line profile of Ly α photons is not significantly affected by the I-front propagation.

In the rest frame of the gas, the radiation field is not isotropic due to the Doppler shift of photons, resulting in a net drag force. By considering the anisotropic radiation pressure (Dijkstra & Loeb 2008), the radiation drag in the Ly α radiation field is estimated as

$$F_{\text{drag}} = \frac{4\pi}{c} \int dx \sigma(x) K(x), \quad (9)$$

where

$$K(x) = \int d\mu \mu I(x), \quad (10)$$

with $\mu \equiv \cos\theta$. The cross section is estimated by $\sigma(x) = 1.04 \times 10^{-13} T_4^{-1/2} H(a, x)/\sqrt{\pi}$ (Verhamme et al. 2006).

The change in velocity for a gas cloud due to this drag is then $dV/dt = -F_{\text{drag}}$. In what follows we will show results for the velocity evolution of gas clouds around a Pop III star of $120 M_\odot$ at $z = 20$ as a fiducial case, and study cases with different masses and redshifts. For simplicity we will refer to velocity and angular momentum below and not separately distinguish between tangential and radial veloci-

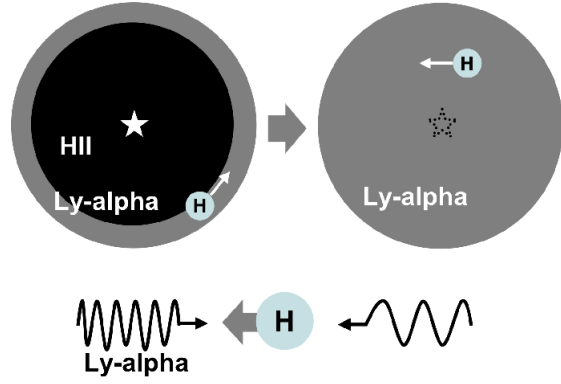


Figure 1. Schematic view of our model. The high-density region of Ly α photons is generated by recombinations in the HII region. Gas can feel higher Ly α radiation pressure to the opposite of the moving direction due to the Doppler shift, resulting in the radiation drag.

ties, and momentum and angular momentum, respectively, as the Ly α field is isotropic and homogenous.

3 RESULTS

Figure 2 shows F_{drag} as a function of gas velocity. The drag force F_{drag} is roughly proportional to the cross section and energy difference due to the Doppler shift, both of which are functions of the relative velocity with respect to the background radiation field. The energy difference of photons by Doppler shift is proportional to $\sim x$, $\Delta E \propto x$. Hence, if $x \ll 1$, and $\sigma \propto e^{-x^2} \sim 1 - x^2$, as a result, $F_{\text{drag}} \propto x \propto v$. On the other hand, if $x \gg 1$, $\sigma \propto x^{-2}$, hence $F_{\text{drag}} \propto x^{-1} \propto v^{-1}$. Therefore, the Ly α radiation drag has a peak near $x \sim 1$. In comparison, radiation drag due to the Compton scattering of continuum radiation is simply proportional to the gas velocity (Umemura et al. 1993). Furthermore, although the absolute value of F_{drag} changes with stellar mass and redshift due to the change in the number density of Ly α photons, the functional shape does not. The shape depends only on the temperature of the gas from which Ly α photons are emitted. In this work, we assume $T = 10^4$ K, as a result the peak is at $V = 17 \text{ km s}^{-1}$. With increasing temperature, the peak position moves to slightly larger velocities. However, the dependence on temperature is not significant in the range of $10^4 \leq T \leq 3 \times 10^4$ K which is the typical temperature of HII region. For $T = 10^4$ K and $n_{\text{Ly}\alpha} = 2.5 \times 10^{-3} \text{ cm}^{-3}$ (the case of $M_{\text{PopIII}} = 120 M_\odot$ at $z = 20$), we can roughly fit the drag force by $F_{\text{drag}} = 0.4 \times 10^{-32} \text{ erg cm}^{-1} (v/1 \text{ km s}^{-1})$ if $v < 17 \text{ km s}^{-1}$, and $F_{\text{drag}} = 0.4 \times 10^{-31} \text{ erg cm}^{-1} (v/20 \text{ km s}^{-1})^{-1}$ if $v > 17 \text{ km s}^{-1}$. For different number densities $n_{\text{Ly}\alpha}$ the drag force can be estimated scaling these fits linearly with the number density.

The initial mass function of Pop III stars is still under debate, it likely depends on the environment of the formation site. Recently, Hirano et al. (2013) carried out a large set of cosmological hydrodynamics simulations following 100 Pop III stars forming, and suggested that the mass of Pop III stars might range from ~ 10 to $\sim 1000 M_\odot$. To ac-

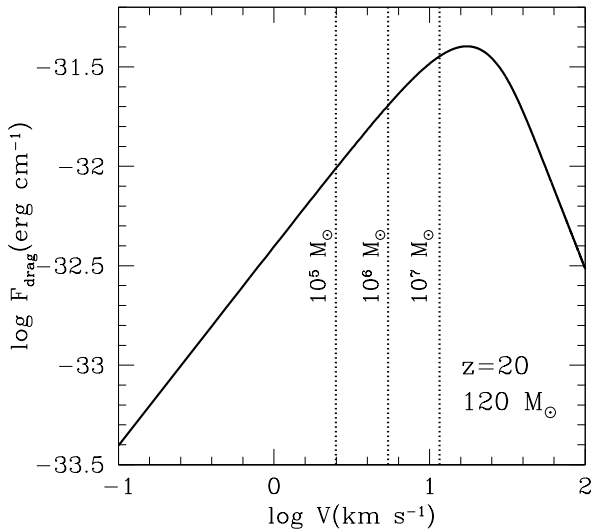


Figure 2. Radiation drag as a function of velocity of gas clouds around a Pop III star of $120 M_{\odot}$ at $z = 20$. Dotted lines show virial velocities of 10^5 , 10^6 and $10^7 M_{\odot}$ halos at $z = 20$.

count for this uncertainty, we here calculate F_{drag} around Pop III stars for a range of masses with the ionizing photon emissivities and life times of Pop III stars taken from Schaerer (2002). The velocity evolution of gas clouds around Pop III stars of 15, 40, 120 and $400 M_{\odot}$ at $z = 20$ are shown in Figure 3. Different line types represent different initial velocities of clouds. As shown in the Figure, there is no clear difference in the velocity evolution for different stellar masses. Since luminosity is linearly proportional to stellar mass and the effective temperature for the stars considered here is almost constant at $T \sim 10^5$ K (Bromm et al. 2001), the ionizing photon emissivity linearly increases with stellar mass $\dot{N}_{\text{Ion}}^{\gamma} \propto M_{\text{PopIII}}$. As shown in equation (1) and (2), $V_{\text{HII}} = R_{\text{S}}^3 [1 - \exp(-t_{\text{life}}/\tau_{\text{rec}})] \sim R_{\text{S}}^3 (t_{\text{life}}/\tau_{\text{rec}}) \propto \dot{N}_{\text{Ion}}^{\gamma} t_{\text{life}}$. Therefore, $n_{\text{Ly}\alpha} \propto \dot{N}_{\text{Ion}}^{\gamma} t_{\text{life}}/V_{\text{HII}} \sim \text{const}$ and hence the Ly α radiation drag does not depend on stellar mass.

Clouds with $V_{\text{init}} = 10 \text{ km s}^{-1}$ lose half of their angular momentum at $t = 1.0 \times 10^6 \text{ yr}$, and move with $V = 0.1 \text{ km s}^{-1}$ at $t = 6.0 \times 10^6 \text{ yr}$. Gas clouds with $V_{\text{init}} = 20$ and 30 km s^{-1} are beyond the peak in F_{drag} but have somewhat higher drag forces acting on them than those at $V = 10 \text{ km s}^{-1}$. These clouds pass through the peak of F_{drag} in their velocity evolution, and hence the time-averaged F_{drag} is higher than that of clouds starting out at $V_{\text{init}} = 10 \text{ km s}^{-1}$. As a consequence, although their initial angular momenta are higher, the time scale required to reach $V = 0.1 \text{ km s}^{-1}$ is only slightly larger to that of $V_{\text{init}} = 10 \text{ km s}^{-1}$. For gas with $V_{\text{init}} = 100 \text{ km s}^{-1}$, the velocity evolution is very slow, and becomes $V = 0.1 \text{ km s}^{-1}$ at $t = 6.6 \times 10^7 \text{ yr}$ which is comparable to the recombination time scale at $z = 20$. After recombination of the IGM, the mean free path of Ly α photons becomes much shorter, and their frequency can quickly change to the red wing part, resulting in an escape from the local region and a drop in the number density of Ly α photons. In effect only gas with

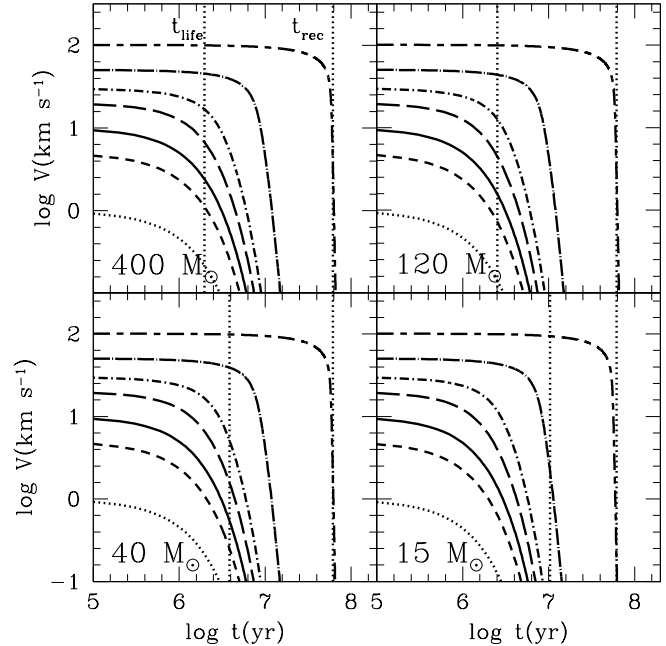


Figure 3. Time evolution of the gas velocity of a neutral gas cloud in a Ly α radiation field generated around Pop III stars at $z = 20$. Different line types represent different initial velocities of the cloud. Vertical dotted lines are life times of stars and a recombination time scale at $z = 20$.

$V_{\text{init}} \lesssim 100 \text{ km s}^{-1}$ lose a significant fraction of its angular momentum.

The circular velocities of dark matter haloes of 10^6 and $10^7 M_{\odot}$ at $z = 20$ are corresponding to 5.4 and 11.6 km s^{-1} respectively. The peak velocity of F_{drag} is corresponding to haloes with circular velocity of $3 \times 10^7 M_{\odot}$ at $z = 20$ and $9 \times 10^7 M_{\odot}$ at $z = 10$. In the current standard scenario, Pop III stars form in mini-halos of $\sim 10^6 M_{\odot}$ at $z \sim 20$ (e.g., Yoshida et al. 2008), subsequently evolving into the first galaxies with $\sim 10^8 M_{\odot}$ at $z \sim 10$ (e.g., Wise et al. 2012) via gas accretion and mergers. Given that the time scale associated with the loss of angular momentum is shorter than the dynamical time scale at $z = 20$ we expect this effect to impact the growth from the first stars to the first galaxies.

Please note that we here assume a uniform IGM density field in which the photon drag takes place. This is justified outside the virial radius of the halo. We have neglected the interaction within the virial radius which is subject to complex geometry and physical state of the gas. However, the size of the HII region is ~ 10 times larger than the typical virial radius ($V_{\text{halo}}/V_{\text{HII}} \sim 10^{-3}$), and most of the angular momentum will be lost during the phase outside the virial radius.

As well as having a wide range of stellar mass, Pop III stars can form at various redshifts (Wise et al. 2012). Figure 4 shows the velocity evolution at different redshifts. With decreasing redshift, F_{drag} decreases, resulting in slower velocity change. The Hydrogen number density of the IGM increases with redshift as $(1+z)^3$, resulting in $R_{\text{S}} \propto (1+z)^{-2}$. In addition, with decreasing gas density, the recombination time scale becomes larger, $\tau_{\text{rec}} \sim 1/(\alpha_{\text{B}} n_{\text{H}}(z))$ leading

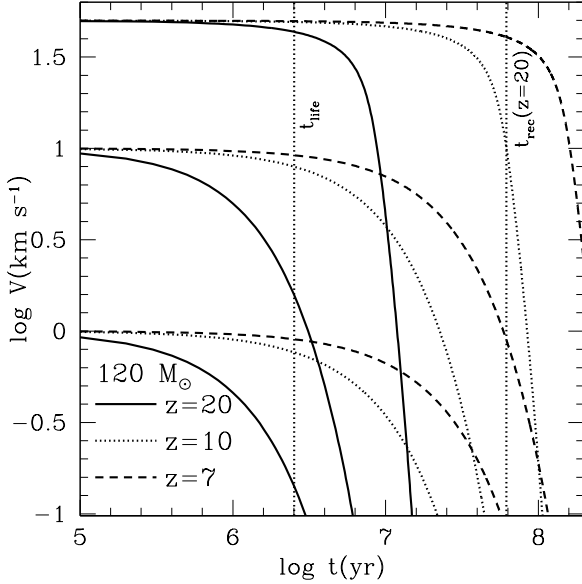


Figure 4. Time evolution of gas cloud velocities in $\text{Ly}\alpha$ radiation field surrounding a Pop III star of $120 M_{\odot}$ at different redshifts. Vertical dotted lines are a life time of star and a recombination time scale at $z = 20$.

to $R_I = R_S(1 - \exp(-t_{\text{life}}/\tau_{\text{rec}}))^{1/3} \sim R_S(t_{\text{life}}/\tau_{\text{rec}})^{1/3} \propto n_{\text{H}}^{-1/3} \propto (1+z)^{-1}$. As a result, F_{drag} changes with redshift as $(1+z)^3$ because of $n_{\text{Ly}\alpha} \propto V_{\text{HII}}^{-1}$. At $z = 7$, it takes 1.2×10^8 yr until a cloud with $V_{\text{init}} = 10 \text{ km s}^{-1}$ slows down to 0.1 km s^{-1} , which is longer than the recombination time scale. This effectively limits the $\text{Ly}\alpha$ photon drag to high redshifts ($z > 7$) even for $V_{\text{init}} \lesssim 10 \text{ km s}^{-1}$.

In this work, our model assumes HII regions are surrounded by a neutral IGM, however, HII bubbles in the IGM can overlap with each other at later redshifts. In this case the distance that $\text{Ly}\alpha$ photons travel to residual HI boundaries is much larger and the scattering cross section is lower due to the Hubble flow. For example, Iliev et al. (2006) show the size of overlapping HII bubbles around galaxies can be $\gtrsim 10$ Mpc. Hence, as HII bubbles overlap, the relative velocity of the HI boundary is much larger than the typical velocity width of the $\text{Ly}\alpha$ line. At this point most of $\text{Ly}\alpha$ photons escape from the large HII bubble without scattering, and the $\text{Ly}\alpha$ radiation drag is no longer effective.

To gain further insight into the effect of the trapping time onto the $\text{Ly}\alpha$ photon drag, we consider that after the death of stars, ionized hydrogen starts to recombine within HII regions. Once the neutral fraction increases, the mean free path of $\text{Ly}\alpha$ photons become shorter as a result of which they can quickly move to energies in the wing of the line profile (Eq. 7) and escape, resulting in smaller trapping times. Adams (1975) showed the mean trapping times from optically-thick clouds with uniform density are $t_{\text{trap}} \sim 15t_{\text{cross}}$. We investigate the impact of the different trapping time on the momentum loss using $t_{\text{trap}} = 15t_{\text{cross}}$ with $t_{\text{cross}} = 2R_I/c$. Figure 5 shows the velocity evolution of gas around Pop III stars at $z = 20$. The boundaries of the shaded regions indicates the velocity evolutions with $t_{\text{trap}} = t_{\text{life}}$ and $t_{\text{trap}} = 15t_{\text{cross}}$. In the case of $120 M_{\odot}$, F_{drag}

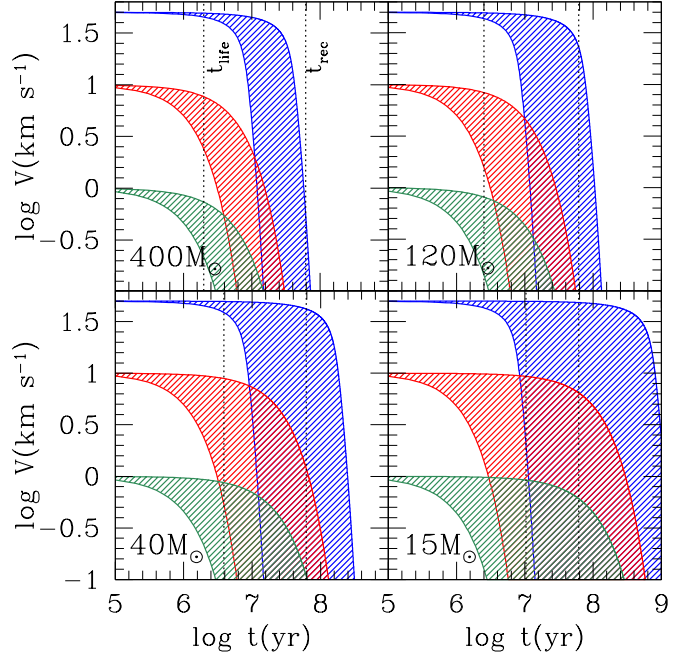


Figure 5. Time evolution of gas cloud velocity in a $\text{Ly}\alpha$ radiation field around Pop III stars at $z = 20$. The upper and lower values in the shaded regions correspond to the cases of $t_{\text{trap}} = 15t_{\text{cross}}$ and $t_{\text{trap}} = t_{\text{life}}$ respectively, where t_{trap} is the trapping time of $\text{Ly}\alpha$ photons, t_{cross} is the crossing time of the system, and t_{life} is life time of the host star. Dotted lines are life times of stars and a recombination time scale at $z = 20$.

is lower than that of the fiducial model with $t_{\text{trap}} = t_{\text{life}}$ by a factor $t_{\text{life}}/(15t_{\text{cross}}) = 8.9$. As a result the velocity of the gas reduces only slowly. The velocity of gas clouds with $V_{\text{init}} = 10 \text{ km s}^{-1}$ becomes half at $t = 0.9 \times 10^7$ yr and 0.1 km s^{-1} at $t = 5.6 \times 10^7$ yr for $120 M_{\odot}$. For high-velocity gas of $V_{\text{init}} = 50 \text{ km s}^{-1}$, the velocity evolution is even slower, and the velocity becomes 0.1 km s^{-1} at $t = 1.3 \times 10^8$ yr.

In addition, as shown in Figure 5, the velocity evolution in the case of $t_{\text{trap}} = 15t_{\text{cross}}$ significantly depends on stellar mass. With decreasing stellar mass, F_{drag} becomes lower and hence the velocity evolution gets slower. This is because, $R_I \propto N_{\text{Ion}}^{1/3}$, and $V_{\text{HII}} \propto R_I^3$ and $t_{\text{trap}} \propto R_I$, as a result, $F_{\text{drag}} \propto \dot{N}_{\text{Ion}}^{\gamma} R_I / V_{\text{HII}} = M_{\text{PopIII}}^{1/3}$. For a $400 M_{\odot}$ star a gas cloud with $V_{\text{init}} = 10 \text{ km s}^{-1}$ loses half of initial angular momentum at $t = 5.0 \times 10^6$ yr and becomes $V = 0.1 \text{ km s}^{-1}$ at $t = 3.0 \times 10^7$ yr. On the other hand, for a $15 M_{\odot}$ star, it takes 9.5×10^7 yr until the initial velocity of 10 km s^{-1} reduces to half that, and 5.8×10^8 yr until it is 0.1 km s^{-1} .

Figure 6 shows the time by which gas has lost half of its initial velocity (t_{half}). Depending on the situations, t_{half} changes, and ranges between $\sim 1 \times 10^6$ to $\sim 2 \times 10^7$ yr for $V \lesssim 20 \text{ km s}^{-1}$. For $V \lesssim 20 \text{ km s}^{-1}$, t_{half} is almost constant, because F_{drag} is roughly proportional to V . For $V_{\text{init}} > 20 \text{ km s}^{-1}$, t_{half} steeply increases with the initial velocity, it becomes ~ 1 Gyr at $V_{\text{init}} \gtrsim 100 \text{ km s}^{-1}$ and becomes larger than the recombination time scale. After recombination, $\text{Ly}\alpha$ photons can quickly escape from local regions, resulting in a smaller trapping time. Therefore, for

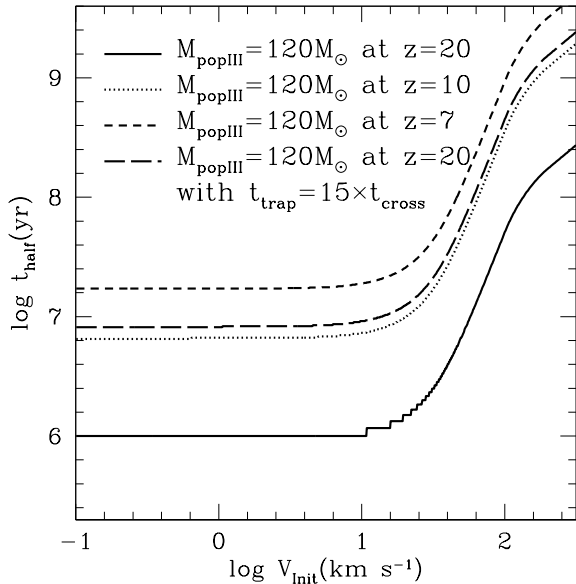


Figure 6. Time scale until the initial velocity becomes half. Different line types are corresponding to different situations. Solid, dot and dash line represent the models for $M_{\text{PopIII}} = 120 M_{\odot}$ at $z = 20, 10$ and 7 respectively. Long dash line shows the model for $M_{\text{PopIII}} = 120 M_{\odot}$ at $z = 20$ with a photon trapping time of 15 times the crossing time.

$V_{\text{init}} \gtrsim 100 \text{ km s}^{-1}$, our estimation of F_{drag} at $t > t_{\text{rec}}$ should be considered an upper limit, and the time scale should be longer.

4 DISCUSSION & SUMMARY

In this paper, we have investigated the effect of radiation drag due to Ly α scattering on accreted neutral gas clouds around first stars. We find that half of the angular momentum of gas with $v_c \lesssim 10 \text{ km s}^{-1}$ near a Pop III star of $120 M_{\odot}$ at $z = 20$ is lost within $\sim 10^6$ yr. Due to the sensitivity of the scattering cross section to gas velocities, the Ly α radiation drag (F_{drag}) declines strongly for gas clouds with velocities $\gtrsim 20 \text{ km s}^{-1}$. For initial gas cloud velocities of 100 km s^{-1} , more than half of the angular momentum can be kept for 5.1×10^7 yr against the radiation drag. For our fiducial model with $t_{\text{trap}} = t_{\text{life}}$, F_{drag} does not depend on stellar mass. On the other hand, F_{drag} is sensitive to redshift. At decreasing redshifts, due to larger sizes of HII regions, the number density of Ly α photon decreases. Consequently, F_{drag} decreases with $(1+z)^3$. We find that only at redshifts $z > 10$, the Ly α radiation drag suppress circular motion of accreted gas efficiently, while it is not likely to block infalling stream motion like cold accretion with $V \gtrsim 100 \text{ km s}^{-1}$ (Yajima et al. 2012c). The radiation drag time-scale is much shorter than that of the dynamical friction in gas medium (Ostriker 1999) and the dynamical time scale at $z \sim 20$. Hence, this effect dominates the angular momentum transport and suppress the formation of large scale gas discs around the first objects like Pop III stars and seed black holes, and enhance the gas accretion towards them. Note that, however, if the clouds enter the

virial radius before the stars die, they are most likely destroyed due to photoevaporation and no accretion onto the central object will occur.

Here, we focused on the gas accretion onto mini haloes in which Pop III stars formed. Similar Ly α radiation drag may occur around the first galaxies at later times. Since the typical formation epoch is later than that of Pop III stars, the Ly α photon density and F_{drag} are smaller. However, recent simulations have shown that the escape fraction of ionizing photons decreases with halo mass (Yajima et al. 2011, 2012d; Paardekooper et al. 2013). Smaller escape fractions result in compact HII regions and high-density Ly α photon fields, resulting in higher F_{drag} . In addition, continuous star formation keeps the production of Ly α photons ongoing and allows the radiation drag to occur for a longer time. Hence, the situation with respect to the Ly α radiation drag around first galaxies is not certain.

After the death of stars, the central region in the HII recombines fast, resulting in a HII shell in between a central HI region and an outer HI border. The shell becomes smaller as the central region continues to recombine while the number of Ly α photons in the shell stays roughly constant. The radiation drag increases during this period in the shell, until it has recombined or the Ly α photons have escaped.

While the assumption of a uniform IGM density is fair, the gas within the virial radius is highly inhomogeneous (Abel et al. 2007). This limits the validity of our model from the edge of the HII region (\sim a few kpc) to the virial radius (\sim a few hundreds pc). However, as we show above this is the dominant region in which angular momentum loss occurs. The evolution inside the halo is complex as e.g. shock waves exist with $\gtrsim 10 \text{ km s}^{-1}$ (Abel et al. 2007; Yoshida et al. 2007). These are generated in tandem with the I-front. At first, due to the high-density gas around the star, the I-front is D-type and slowly propagates with the shock. Then, reaching low-density regions, the I-front changes to R-type and quickly expands, while the shock is left behind stagnating at a propagation velocity of $\gtrsim 10 \text{ km s}^{-1}$. As a result, the shock is at around the virial radius when the central star dies (Yoshida et al. 2007). Once the clump reaches the virial radius, it is likely to interact with the shock and be compressed and heated up. As a result, the accreted gas may be destroyed or survive by efficient cooling emission (Dekel & Birnboim 2006). This evolution of the accreted gas at $\lesssim R_{\text{vir}}$ is out of the scope of our simple model in this paper.

In this work, as a first step, we use an analytic model to estimate the Ly α radiation drag by estimating the upper limit of the possible Ly α radiation field. It is important to note, that in our model trapping of Ly α photons is key. Once e.g. supernovae efficiently blow out gas, Ly α photons are able to escape the local region and the radiation drag quickly becomes unimportant. In a follow-up study we will investigate the Ly α radiation drag in a more realistic set-up including a self-consistent time evolution within hydrodynamics simulations.

ACKNOWLEDGMENTS

We are grateful to Y. Li and M. Umemura for valuable discussion and comments. We thank the anonymous referee for useful comments.

REFERENCES

- Abel T., Wise J. H., Bryan G. L., 2007, *ApJ*, 659, L87
 Adams T. F., 1975, *ApJ*, 201, 350
 Agarwal B., Davis A. J., Khochfar S., Natarajan P., Dunlop J. S., 2013, *MNRAS*, 432, 3438
 Agarwal B., Khochfar S., Johnson J. L., Neistein E., Dalla Vecchia C., Livio M., 2012, *MNRAS*, 425, 2854
 Bromm V., Kudritzki R. P., Loeb A., 2001, *ApJ*, 552, 464
 Bromm V., Yoshida N., 2011, *ARA&A*, 49, 373
 Bryan G. L., Norman M. L., 1998, *AJ*, 495, 80
 Dekel A., Birnboim Y., 2006, *MNRAS*, 368, 2
 Di Matteo T., Khandai N., DeGraf C., Feng Y., Croft R. A. C., Lopez J., Springel V., 2012, *ApJ*, 745, L29
 Dijkstra M., Loeb A., 2008, *MNRAS*, 391, 457
 Dijkstra M., Kramer R., 2012, *MNRAS*, 424, 1672
 Faucher-Giguère C.-A., Kereš D., 2011, *MNRAS*, 412, L118
 Harrington J. P., 1973, *MNRAS*, 162, 43
 Hasegawa K., Umemura M., Susa H., 2009, *MNRAS*, 395, 1280
 Heger A., Woosley S. E., 2002, *ApJ*, 567, 532
 Hirano S., Hosokawa T., Yoshida N., Umeda H., Omukai K., Chiaki G., Yorke H. W., 2013, arXiv: 1308.4456
 Hui L., Gnedin N. Y., 1997, *MNRAS*, 292, 27
 Iliev I. T., Mellema G., Pen U.-L., Merz H., Shapiro P. R., Alvarez M. A., 2006, *MNRAS*, 369, 1625
 Khochfar S., Silk J., 2011, *MNRAS*, 410, L42
 Kitayama T., Yoshida N., Susa H., Umemura M., 2004, *ApJ*, 613, 631
 Laursen P., Duval F., Östlin G., 2013, *ApJ*, 766, 124
 Laursen P., Razoumov A. O., Sommer-Larsen J., 2009, *ApJ*, 696, 853
 Loeb A., 1993, *ApJ*, 403, 542
 Loeb A., Rybicki G. B., 1999, *ApJ*, 524, 527
 Osterbrock D. E., Ferland G. J., 2006, *Astrophysics of gaseous nebulae and active galactic nuclei*, Osterbrock, D. E. & Ferland, G. J., ed. CA: University Science Books
 Ostriker E. C., 1999, *ApJ*, 513, 252
 Paardekoooper J.-P., Khochfar S., Dalla Vecchia C., 2013, *MNRAS*, 429, L94
 Pawlik A. H., Milosavljević M., Bromm V., 2011, *ApJ*, 731, 54
 Pawlik A. H., Schaye J., van Scherpenzeel E., 2009, *MNRAS*, 394, 1812
 Poynting J. H., 1903, *MNRAS*, 64, A1
 Prochaska J. X., O’Meara J. M., Worseck G., 2010, *ApJ*, 718, 392
 Rahmati A., Pawlik A. H., Raičević M., Schaye J., 2013a, *MNRAS*, 430, 2427
 Rahmati A., Schaye J., Pawlik A. H., Raičević M., 2013b, *MNRAS*, 431, 2261
 Raičević M., Pawlik A. H., Schaye J., Rahmati A., 2013, arXiv: 1311.0182
 Robertson H. P., 1937, *MNRAS*, 97, 423
 Romano-Díaz E., Choi J.-H., Shlosman I., Trenti M., 2011, *ApJ*, 738, L19
 Schaerer D., 2002, *A&A*, 382, 28
 Spitzer L., 1978, *Physical processes in the interstellar medium*, Spitzer, L., ed.
 Strömgren B., 1939, *ApJ*, 89, 526
 Susa H. and Umemura M., 2006, *ApJ*, 645, L93
 Susa H., Umemura M., Hasegawa K., *ApJ*, 702, 480
 Tasitsiomi A., 2006, *ApJ*, 648, 762
 Umemura M., Loeb A., Turner E. L., 1993, *ApJ*, 419, 459
 Umemura M., Susa H., Hasegawa K., Suwa T., Semelin B., 2012, *Prog. Theor. Exp. Phys.*, 01A306
 Verhamme A., Schaerer D., Maselli A., 2006, *A&A*, 460, 397
 Whalen D., Abel T., Norman M. L., 2004, *ApJ*, 610, 14
 Wise J. H., Turk M. J., Norman M. L., Abel T., 2012, *ApJ*, 745, 50
 Yajima H., Choi J.-H., Nagamine K., 2011, *MNRAS*, 412, 411
 Yajima H., Li Y., 2013, arXiv: 1308.0381
 Yajima H., Li Y., 2012a, arXiv: 1211.0088
 Yajima H., Li Y., Zhu Q., Abel T., 2012b, *MNRAS*, 424, 884
 Yajima H., Li Y., Zhu Q., Abel T., 2012c, arXiv: 1211.0014
 Yajima H., Li Y., Zhu Q., Abel T., Gronwall C., Ciardullo R., 2012d, arXiv: 1209.5842
 Yajima H., Choi J.-H., Nagamine K., 2012e, *MNRAS*, 427, 2889
 Yoshida N., Oh S. P., Kitayama T., Hernquist L., 2007, *ApJ*, 663, 687
 Yoshida N., Omukai K., Hernquist L., 2008, *Science*, 321, 669